PCCP
Physical Chemistry Chemical Physics

Accepted Manuscript

This article can be cited before page numbers have been issued, to do this please use: G. Che, Y. Fei, X. Tang, Z. Zhao, T. Hattori, J. Abe, X. Wang, J. Ju, D. Xiao, Y. Wang, K. Li and H. Zheng, *Phys. Chem. Chem. Phys.*, 2024, DOI: 10.1039/D4CP03751K.

View Article Online
DOI: 10.1039/D4CP03751K

ARTICLE

Pressure-induced polymerization of 1,4-difluorobenzene towards fluorinated diamond nanothreads

Received 00th January 20xx,
Accepted 00th January 20xx

DOI: 10.1039/x0xx00000x

Guangwei Che, [a] Yunfan Fei, [a] Xingyu Tang, [a] Zilin Zhao,[a] Takanori Hattori, [b] Jun Abe, [c] Xiaoge Wang, [d] Jing Ju, [d] Xiao Dong, [e] Yajie Wang,*[a] Kuo Li, [a] and Haiyan Zheng *[a]

Pressure-induced polymerization (PIP) of aromatic molecules has emerged to be an effective method for synthesizing various carbon-based materials. The selection of suitable functionalized molecular precursors is crucial for obtaining the desired structures and functions. In this work, 1,4-difluorobenzene (1,4-DFB) was selected as the building block for PIP. In situ high-pressure investigations of 1,4-DFB reveals a phase transition at approximately 12.0 GPa and an irreversible chemical reaction at 18.7 GPa. Structural analysis of the product and the kinetics of the reaction uncovered the formation of pseudo-hexagonal stacked fluoro-diamond nanothreads with linear growth. Compared to the crystal structures of benzene under high pressure, 1,4-DFB exhibits higher compression along the $[001]$ axis. The anisotropic compression is attributed to the stronger H···π interaction along the $[01\bar{1}]$ axis and the potential compression-inhibiting H···F interactions along the $[100]$ and $[010]$ axes, and it facilitates a possible reaction pathway along the $[01\bar{1}]$ axis. This work emphasizes the crucial role of functionalization in modulating molecular stacking and influencing the reaction pathway.

Introduction

Pressure-induced polymerization (PIP) of aromatics has been unequivocally established as a highly efficacious strategy for the synthesis of novel carbon materials.[1-3] In 2015, diamond nanothreads (DNTh) were first synthesized through the slow compression of benzene.[4] However, the comparable reactivity of carbon atoms in benzene give rise to several competing bonding pathways during the polymerization process.[5,6] Notable pathways include [4+2] cycloaddition along the $[100]$ and $[010]$ axes and *para*-polymerization along the $[01\bar{1}]$ axis. The competition results in a range of connectivity patterns and contributes to a reduction in the structural order within the intrathread.[6,7]

One strategy to achieve intrathread-ordered DNTh is to incorporate inert heteroatoms into the aromatic ring, examples being furan,[8] thiophene[9] and pyridazine[10] et al.. However, this reduces the number of interunit bonds, leading to weaker mechanical properties.[11] Another viable approach is functionalizing the monomers, like introducing fluorine atoms which can result in the columnar stacking instead of the herringbone-type stacking. Furthermore, the obvious difference of the electronegativity between the hydrogen and fluorine atoms may enhance the reaction selectivity and then results in ordering DNTh. Due to the inverse polarity relationship between the aromatics and perfluoroaryl derivatives, including the 1:1 naphthalene-octafluoronaphthalene[12,13] and anthracene-octafluoronaphthalene[13] cocrystal, both of them are π···π stacked in column, which facilitates the formation of interthread-ordered DNTh. Similarly, a 1:1 phenol-pentafluorophenol[14] cocrystal also displays stable columnar π···π stacking as a result of arene···perfluoroarene interactions, forming DNTh under high pressure. However, the smallest aromatic rings, benzene-hexafluorobenzene cocrystal, undergoes a transformation into tilted columns of π···π stacking under high pressure, producing a two-dimensional (2D) H-F-substituted graphane instead of DNTh.[15,16] All the literatures remind us that high-pressure reactions involving fluorinated aromatics remain highly complex and further investigations are still needed. In this paper, we focused on the partially fluorinated aromatic molecule 1,4-difluorobenzene (1,4-DFB). A phase transition and a reaction were discovered around 12.0 and 18.7 GPa, respectively. The product was identified as pseudo-hexagonal stacked fluorinated DNTh with a *d*-spacing of 6.1 Å, supported by kinetic analysis of its one-dimensional growth. By investigating the crystal structure of 1,4-DFB at 9.4 GPa and comparing it to that of benzene, we observed the greatest compression along the $[001]$ axis as well as a shorter nearest neighbour C···C distance along the $[01\bar{1}]$ axis ($d_{C\cdots C[01\bar{1}]}$). These findings reveal an anisotropic compression under high pressure, which favours a possible reaction pathway along the $[01\bar{1}]$ axis for 1,4-DFB, highlighting the potential of

[a] Center for High Pressure Science and Technology Advanced Research, Beijing 100193, P. R. China. E-mail: yajie.wang@hpstar.ac.cn; zhenghy@hpstar.ac.cn
[b] J-PARC Center, Japan Atomic Energy Agency, Tokai, Ibaraki 319-1195, Japan.
[c] Neutron Science and Technology Center, Comprehensive Research Organization for Science and Society, Tokai, Ibaraki 319-1106, Japan.
[d] College of Chemistry and Molecular Engineering, Peking University, Beijing 100871, P. R. China.
[e] Key Laboratory of Weak-Light Nonlinear Photonics, School of Physics, Nankai University, Tianjin 300071, P. R. China.

Supplementary Information available: Raman and IR decompression spectra of 1,4-DFB (Fig. S1); IR spectra of samples recovered from 17.5 and 18.7 GPa (Fig. S2); Rietveld refinement plot and the structure of 1,4-DFB at 4.3 GPa (Fig. S3); crystal structures of 1,4-DFB at 9.4 GPa and d_6-benzene at 9.2 GPa along the $[010]$, $[\mathbf{10}0]$ and $[\mathbf{80}3]$ axes, respectively (Fig. S4); a schematic diagram of the proposed packing of product (Fig. S5); the experimental Raman results (4.2 GPa, room temperature) and the calculated data (4.3 GPa, 0 K) with corresponding vibrational assignments (Table S1); the experimental IR results (4.3 GPa, room temperature) and the calculated data (4.3 GPa, 0 K) with the assignments (Table S2); atomic coordinates of 1,4-DFB at 4.3 GPa (Table S3); atomic Coordinates of 1,4-DFB at 9.4 GPa (Table S4). atomic coordinates of benzene at 9.2 GPa (Table S5). See DOI: 10.1039/x0xx00000x

functionalization for designing and synthesizing new carbon materials.

Experimental

1,4-difluorobenzene (>98.0%, GC purity grade) was purchased from *Meryer (Shanghai) Chemical Technology Co., Ltd.* and used without further purification. Symmetric diamond anvil cells (DACs) with the anvil culet of 300 μm in diameter were used for the in situ high-pressure Raman, *mid*-IR and XRD experiments. T-301 stainless steel gaskets were pre-indented to a thickness of 30 μm, and a predrilled hole with a diameter of 100 μm served as the sample chamber. The pressure was determined using the fluorescence peak of the ruby.[17] For all in situ experiments, we didn't use the pressure medium. For in situ Raman and synchrotron X-ray diffraction, 1,4-DFB was cryogenically loaded into the DAC in liquid nitrogen. The sample was quickly sealed to form powder-crystal and prevent the formation of large grains or preferred orientation.

For in situ IR experiments, a pair of type II diamonds were used. Bruker VERTEX 70v with HYPERION 2000 microscope was used with a Globar as a conventional source. The spectra were collected in a transmission mode in the range of 600 – 4000 cm^{-1} with a resolution of 2 cm^{-1} through a 40 × 40 μm^2 aperture. KBr was used to dilute 1,4-DFB in the sample chamber to prevent the signal from exceeding the detection limit. An appropriate amount of dried and ground KBr was placed into the sample chamber and then pre-pressed into thin slice, after which liquid 1,4-DFB was added. The sample chamber was then sealed quickly to prevent the evaporation of 1,4-DFB. The absorption of the diamond anvils loaded with KBr in the aperture region was used as the background. For the in situ Raman experiment, a commercial Renishaw Raman microscope (RM1000) with the laser wavelength of 532 nm was used. The silicon line at 520 cm^{-1} was used to calibrate system before measurements.

In situ synchrotron X-ray diffraction data under high pressure were collected at the 4W2 beamline of the Beijing Synchrotron Radiation Facility (BSRF). The wavelength of incident monochromatic X-ray was 0.6199 Å and the beam size was 20 × 30 μm^2. The CeO_2 standard sample was used to calibrate the Pilatus detector. The collected data was reduced by Dioptas software.[18]

To explore the influence of introducing fluorine atoms on molecular stacking and reaction pathways, we compared the crystal structure of 1,4-difluorobenzene (DFB) with that of benzene under similar high-pressure conditions. We conducted an in situ time-of-flight (TOF) neutron diffraction experiment on benzene at 9.2 GPa. Benzene (d_6, 100%, isotopic) was purchased from *Alfa Aesar,* and used for the in situ TOF neutron diffraction experiment without further purification. In situ TOF neutron diffraction experiment was conducted at BL11 PLANET in the Materials and Life Science Experimental Facility (MLF) at the Japan Proton Accelerator Research Complex (J-PARC).[19] A VX4 Paris-Edinburgh Press equipped with double-toroidal sintered diamond anvils and a Titanium-Zirconium (TiZr) alloy gasket (cup diameter of 3 mm) was used for compressing 1,4-DFB. An automatic hydraulic oil syringe pump was used for driving the system, and the pressure was estimated using the PLANET group calibration curve.[20] A mixture of methanol and ethanol (4:1) was used as the pressure medium, and the mixed ratio between pressure medium and benzene-d_6 was 1:7.5. The sample was loaded into the gaskets at low temperature created with liquid nitrogen.

In ex situ experiments, 1,4-DFB was cryogenically loaded into the DAC and then compressed to 30.0 GPa. The recovered product was subsequently used for structural investigation. Selected area electron diffraction patterns were recorded using a JEOL-2100 transmission electron microscope at 80 kV under low-temperature conditions.

Density functional theory (DFT) calculations were performed to calculate Raman and IR spectra in Cambridge Sequential Total Energy Package (CASTEP) module[21] in Material Studio. The local density approximation (LDA) exchange correlation function by Ceperley and Alder was parameterized by Perdew and Zunger (CA-PZ)[22], then it was used to generate on the fly (OTFG) norm conserving pseudopotentials with an energy cutoff of 840 eV. The k-points solution was 2π * 0.04 $Å^{-1}$. The non-covalent interaction was described by DFT-D correction forwarded by Ortmann, Bechstedt, and Schmidt.[23]

Results and discussion

In situ spectroscopic investigation under high pressure

The high-pressure behavior of 1,4-DFB was investigated by in situ Raman spectroscopy up to 21.2 GPa at room temperature. Figure 1a illustrates the evolution of the Raman spectra under high pressure. The assignment of Raman peaks was shown in Table S1, referencing the simulated results based on the crystal structure and the reports of fluorinated aromatic compounds.[16] Under compression, two peaks appeared at 449 and 458 cm^{-1} in the shoulder of the C-C-C out of plane bending mode at 12.3 GPa as marked by red arrows. Besides, a variation of the Raman shifts with pressure is detected around 10.5 GPa (Fig. 1b), which thus indicated a sluggish phase transition in a wide pressure range from 10.5 to 12.3 GPa. At 15.1 GPa, most of peaks in the lattice mode region almost disappeared, indicating an amorphization before reaction. Above 17.9 GPa, a slower Raman shifts dependent with pressure was observed, which is similar with the phenomenon of the reported benzene case,[24] indicating the beginning of the pressure-induced reaction of 1,4-DFB. The result is also in consistent with the in situ IR and XRD data, that will be discussed later. For the Raman spectra upon decompression (Fig. S1a), the fluorescence background was so strong that it obscured the sample peak, and no new peak was observed during decompression.

In situ *mid*-IR spectra of 1,4-DFB were measured from 1.5 to 30.5 GPa at room temperature. The IR peak assignments based on simulated results and references [25] are presented in Table S2. As shown in Fig. 1c, all peaks showed a blue shift as the pressure increasing and no pronounced spectral changes happened from 1.5 to 12.0 GPa. When compressing 1,4-DFB to 13.9 GPa, a new peak appeared at 851 cm^{-1} in the left shoulder of the C-H out-

View Article Online
DOI: 10.1039/D4CP03751K

ARTICLE

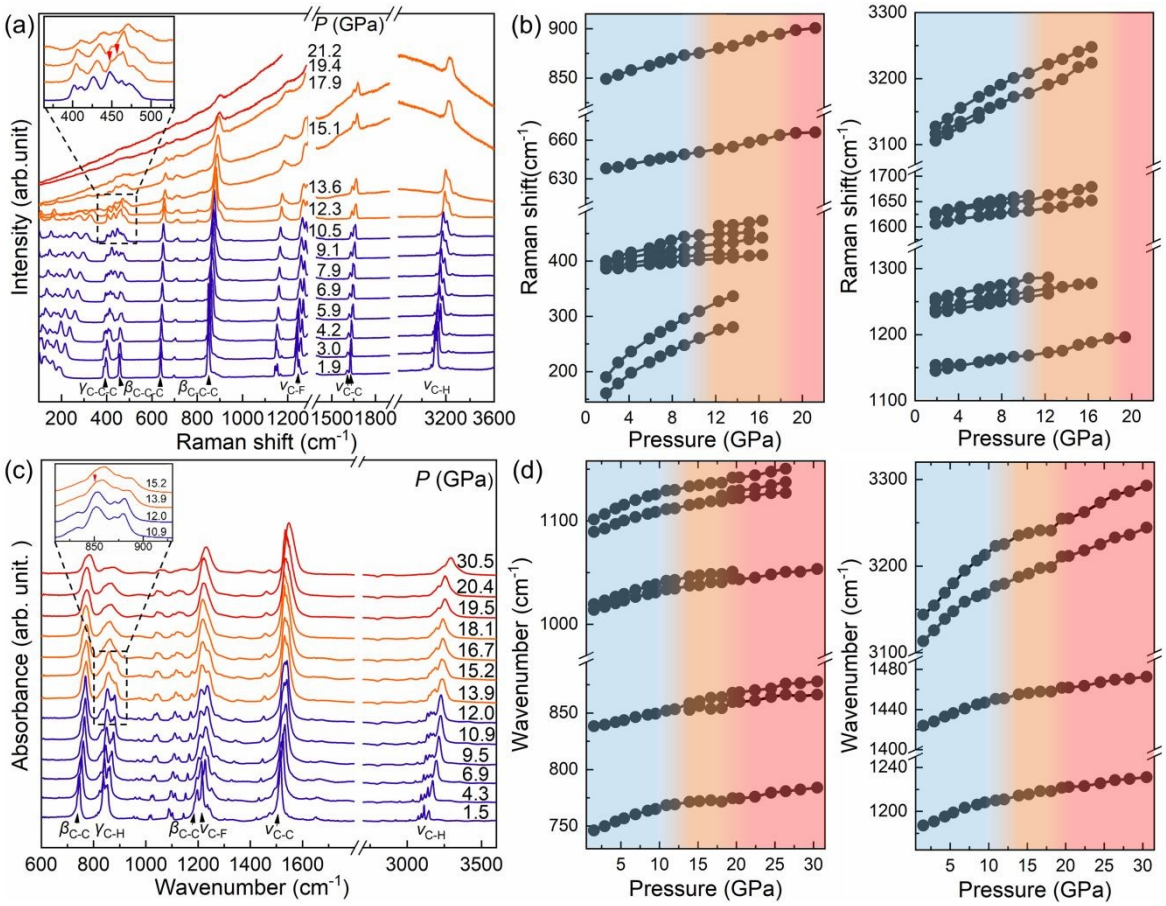

Fig. 1. (a) In situ Raman spectra of 1,4-DFB under high pressure. The omitted range of 1285-1390 cm^{-1} overlapped with the diamond modes and that of 1900-2800 cm^{-1} lacked fundamental vibrational modes. For the spectra of 17.9, 19.4 and 21.2 GPa, a partial signal overflowed because of the enhanced fluorescence signal. *ν*, *γ*, and *β* represent the stretching, out-of-plane bending, and in-plane bending vibration, respectively. (b) Raman shifts of 1,4-DFB as a function of pressure in the range of 150–915 and 1100–3300 cm^{-1}. The different colours represent different phases or chemical reaction. (c) In situ IR spectra of 1,4-DFB upon compression. The spectral range of 1700-2700 cm^{-1} is omitted because of the strong absorbance of the diamonds and the inexistence of peak. The new peaks are marked by red arrows. (d) Wavenumbers of 1,4-DFB as a function of pressure in the range of 730–1160 and 1165–3300 cm^{-1}.

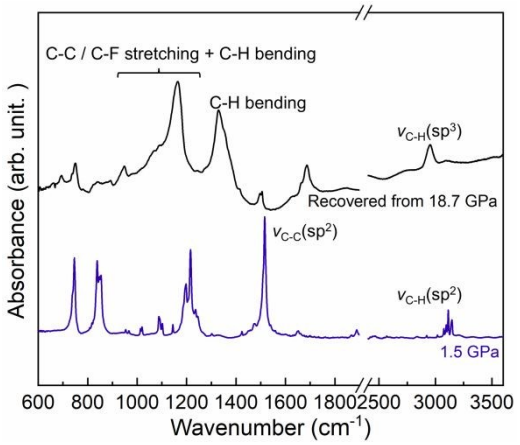

Fig. 2 IR spectra of 1,4-DFB at 1.5 GPa and product recovered from 18.7 GPa. *ν* represents the stretching vibration.

of-plane bending (γ_{C-H}) as shown in the inset of Fig. 1c. Besides, an obvious discontinuity appeared at the dependence of IR modes on pressure around 12.0 GPa (Fig. 1d), thus indicating the pressure-induced phase transition occurring from 12.0 to 13.9 GPa, which is in consistence with Raman result.

When compressing 1,4-DFB to 18.7 GPa, several IR modes show slight discontinuity with pressure, but still survived up to ~30 GPa, (the maximum pressure of the experiment, Fig. 1c and 1d). When we compressed the sample to 18.7 GPa, kept for 12 hours and decompressed to ambient pressure, no obvious new peak appeared (Fig. S1b), but white solid product was obtained. This evidenced the polymerization and can't be observed when recovered from pressure of 17.5 GPa or lower (Fig. S2, raw material was volatilized). After carefully removing the 1,4-DFB by vacuuming for 12 hours, the recovered product was analyzed by IR spectroscopy. As shown in Fig. 2, the peaks of recovered product of C=C stretching (ν_{C-C}) at 1500-1530 cm^{-1} and sp^2 C-H

View Article Online
DOI: 10.1039/D4CP03751K

ARTICLE

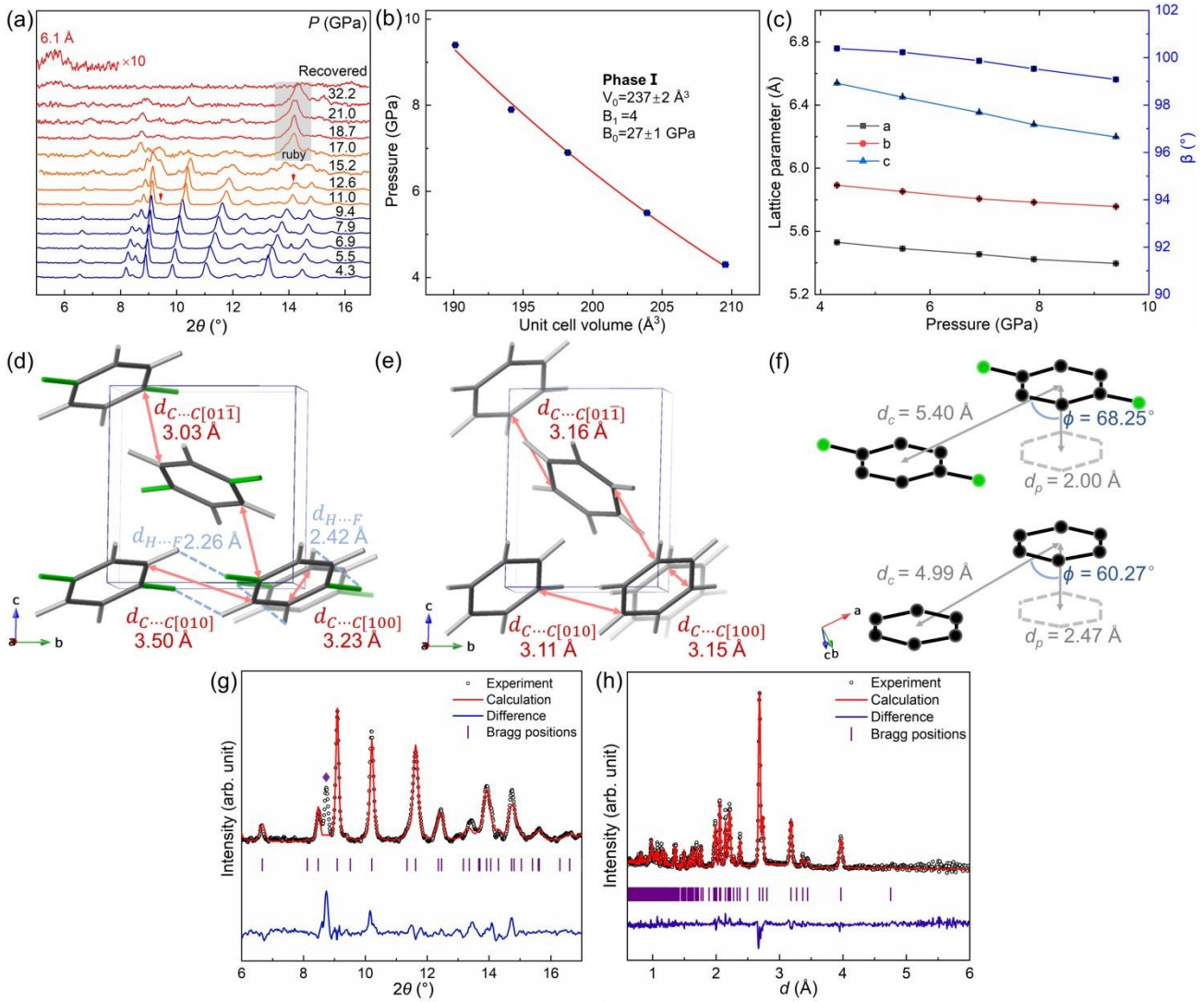

Fig. 3 (a) In situ XRD of 1,4-DFB under high pressure. New peaks after phase transition were marked by red arrows. The ruby diffractions are marked by gray rectangle. (b) Birch–Murnaghan equation of the state of 1,4-DFB under non-hydrostatic pressure conditions. The error bars are smaller than the labels. (c) The evolution of corresponding lattice parameters of 1,4-DFB in the range from 4.3 to 9.4 GPa. The error bars are smaller than the labels. (d) Crystal structures of 1,4-DFB at 9.4 GPa along the $[\mathbf{100}]$ axis, which was determined by Rietveld refinement of in situ XRD data as shown in Fig. 3g. Pink lines show the nearest neighbour C···C distances, for example, the $\boldsymbol{d_{C\cdots C[01\bar{1}]}}$ means the nearest neighbour C···C distance along the $[\mathbf{01\bar{1}}]$ axis. Blue dotted lines show the interactions between H atoms and F atoms. (e) Crystal structures of d_6-benzene at 9.2 GPa along the $[\mathbf{100}]$ axis, which was determined by Rietveld refinement of in situ TOF neutron diffraction data as shown in Fig. 3h. (f) Structures of 1,4-DFB (9.4 GPa) and benzene (9.2 GPa) showing local π-stacking. d_c is the distance between the ring centroids, d_p is the distance between parallel ring planes and ϕ is slippage angle between parallel ring planes. (g) Rietveld refinement plot of 1,4-DFB at 9.4 GPa with R_{wp} at 14.84 %. To construct the complete 1,4-DFB molecule as a rigid body, we changed the space group to $P2_1$ during the refinement process. The peak marked with purple diamond originates from an unknown impurity. (h) Rietveld refinement plot of d_6-benzene at 9.2 GPa with R_{wp} at 21.22 %.

stretching ($\nu_{C\text{-}H}$) at 3017-3143 cm^{-1} disappeared. Additionally, the new peaks observed in the regions of the 1300-1375 cm^{-1} and 2900-2990 cm^{-1} correspond to sp^3 C-H bending ($\delta_{C\text{-}H}$) and sp^3 C-H stretching ($\nu_{C\text{-}H}$) in product, referencing the reports on F-substituted DNThs.[12] These evidenced the polymerization of 1,4-DFB with the formation of an sp^3 carbon material.

In situ X-ray diffraction under high pressure

To investigate the structural variation of 1,4-DFB under high pressure, in situ XRD patterns were collected up to 32.2 GPa (Fig. 3a). The crystal structure of 1,4-DFB of phase I at 4.3 GPa and room temperature was investigated and determined through Rietveld refinement (Fig. S3) with a space group of $P2_1/c$, similar

View Article Online DOI: 10.1039/D4CP03754K

to the low-temperature and ambient pressure crystal structure reported in the literature.[26] Its lattice parameters are a = 5.530(2) Å, b = 5.892(2) Å, c = 6.5384(13) Å, and β = 100.39(3)°, and the atomic coordinates are provided in Table S3. The cell volumes and parameters below 9.4 GPa were obtained from the Rietveld refinement. The unit cell volumes as a function of pressure were fitted by using the third-order Birch–Murnaghan equation of state (EOS)[27]:

$$P(V) = 1.5B_0\left[\left(\frac{V_0}{V}\right)^{\frac{7}{3}} - \left(\frac{V_0}{V}\right)^{\frac{5}{3}}\right] * \{1 + \frac{3}{4}(B_1 - 4)\left[\left(\frac{V_0}{V}\right)^{\frac{2}{3}} - 1\right]\}$$

where V_0 is the unit cell volume at ambient pressure, B_0 and B_1 are the isothermal bulk modulus and its first pressure derivative, respectively. As shown in Fig. 3b, a curve was used to fit the data in the range from 4.3 to 9.4 GPa with B_1 fixed to 4, and the result shows V_0 = 237 ± 2 Å^3, B_0 = 27 ± 1 GPa. The excellent fit indicates no phase transition below 9.4 GPa, consistent with Raman and IR results. Upon continuous compressing, two new peaks appeared at 9.4 and 14.1 ° from 11.0 to 12.6 GPa. Additionally, the diffractions at 11.0 GPa could not be indexed using the lattice parameters of phase I, which indicated a phase transition, corresponding to Raman and IR results. At 15.2 GPa, an amorphization before reaction with the sudden weakening of all peaks was observed. When decompressing from 32.2 GPa to ambient pressure, the recovered product shows a broad and weak peak with d = 6.1 Å, which was very like the diffraction observed at d∼ 5 to 6 Å of DNThs synthesized by the PIP of benzene.[4,5]

As shown in Figure 3d, the crystal structure of 1,4-DFB at 9.4 GPa was obtained by Rietveld refinement of in situ XRD data (Fig. 3g, the atomic coordinates shown in Table S4). In order to understand the influence of introducing fluorine atoms on molecular stacking, the structure of d_6-benzene at 9.2 GPa was also investigated in this work for comparison (Fig. 3e), as determined by Rietveld refinement of TOF neutron data (Fig. 3h, the atomic coordinates shown in Table S5). As shown in Fig. S4, 1,4-DFB shows a herringbone stacking along the $[\mathbf{01\bar{1}}]$ axis and a tilted-column stacking along the $[\mathbf{100}]$ and $[\mathbf{010}]$ axes. The quality of the π-stacking can be quantified by the parameters including slippage angle between parallel ring planes (ϕ), the distance between the ring centroids (d_c) and the distance between parallel ring planes (d_p), proposed by Timothy et al.[28] As shown in Fig. 3f, in 1,4-DFB, the ϕ and d_c are ϕ=68.25° and d_c=5.40 Å, respectively, which are similar to those of benzene (ϕ=60.27°, d_c=4.99 Å). This indicates 1,4-DFB has higher d_c and ϕ as the case in benzene, which means it exhibits "poor" π···π stacking.[28] However, it is worthy to note that in contrast to benzene (II), [29,30] the 1,4-DFB shows more obviously anisotropic compression under high pressure with $[\mathbf{001}]$ axis showing the greatest compression of 5.17%, comparing with compression of $[\mathbf{100}]$ axis (2.58%) and the $[\mathbf{010}]$ axis (2.03%) as shown in Fig. 3c. This anisotropic compression stems from the strong H···π interaction along the $[\mathbf{01\bar{1}}]$ axis and the compression-limiting H···F interaction along the $[\mathbf{100}]$ and $[\mathbf{010}]$ axes (marked by the blue dotted line in Fig. 3d). Along the [**100**] and [**010**] axes the H···F distances are 2.42 and 2.26 Å, respectively. They are all shorter than the sum of the van der Waals radii of F and H atoms (d_{vF} = 1.47 Å, d_{vH} = 1.2 Å), [31] indicating a repulsive interaction. These interactions lead to a shorter nearest neighbour C···C distance along the $[\mathbf{01\bar{1}}]$ axis ($\boldsymbol{d}_{\boldsymbol{C}\cdots\boldsymbol{C}[\mathbf{01\bar{1}}]}$ = 3.103 Å) and longer distances along the $[\mathbf{100}]$ and $[\mathbf{010}]$axes ($\boldsymbol{d}_{\boldsymbol{C}\cdots\boldsymbol{C}[\mathbf{100}]}$ = 3.23 Å, $\boldsymbol{d}_{\boldsymbol{C}\cdots\boldsymbol{C}[\mathbf{010}]}$ = 3.50 Å), instead of the almost identical distances observed in benzene ($\boldsymbol{d}_{\boldsymbol{C}\cdots\boldsymbol{C}[\mathbf{01\bar{1}}]}$ = 3.16 Å, $\boldsymbol{d}_{\boldsymbol{C}\cdots\boldsymbol{C}[\mathbf{100}]}$ = 3.15 Å, $\boldsymbol{d}_{\boldsymbol{C}\cdots\boldsymbol{C}[\mathbf{010}]}$ = 3.11 Å). As a result, a potential reaction pathway along the $[\mathbf{01\bar{1}}]$ axis is favoured for 1,4-DFB.

Structure analysis of the recovered product

The selected area electron diffraction (SAED) pattern of the recovered sample (Fig.4) revealed a pseudo-hexagonal symmetry with d-spacings of 6.1, 5.9, and 6.0 Å, corresponding to the {010} planes in hexagonal lattice. It aligns with the characteristics of DNThs synthesized via the PIP of aromatic molecules,[4,5,8,32] and the d-spacing represents the interplanar distance between the layers formed by DNThs (Figure S5). It is noted that product showed electron irradiation sensitivity with enlarged d-spacing and gradually dispersive diffraction spot, even at the voltage of 80 kV and the temperature of 77 K, consistent with the reports of DNThs synthesized from benzene.[33]

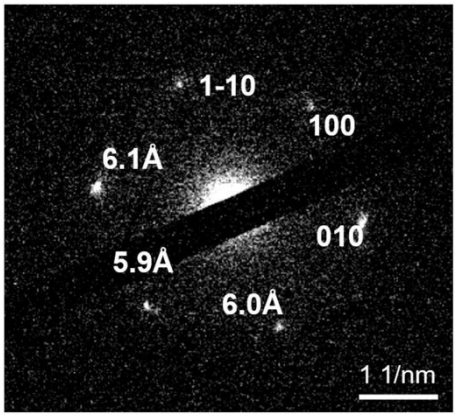

Fig. 4 Selected area electron diffraction (SAED) of the recovered product at the voltage of 80 kV and the temperature of 77 K.

To further analyze the reaction mechanism, the kinetic process of reaction was investigated via collecting IR absorption spectra as a function of time under constant pressure and ambient temperature as shown in Fig. 5. The pressure of 25.5 GPa was chosen because the transformation rate at the onset pressure of the reaction at 18.7 GPa is too slow. Avrami model was used to analyze kinetics of pressure-induced solid–state reactions.[34] The fraction of the reacted 1,4-DFB monomer as a function of time $R(t)$ was fitted using the following relationship:

$$R(t) = \frac{I(0) - I(t)}{I(0)} = R_\infty[1 - e^{[-k(t-t_0)^n]}]$$

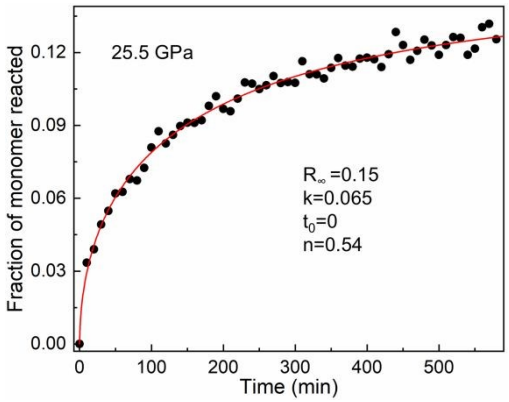

Fig. 5 Kinetic evolution of the reactions at ambient temperature and 25.5 GPa. The fraction of the reacted monomer determined by the absorption of selected main bands, is plotted as a function of time. The fitting parameters are shown in the inset.

where the intensity *I* corresponds to the integration of selected main bands in the region of 1500-1615 cm^{-1}, which serves as an excellent probe to determine the amount of reacted monomer via the attenuated integrated-area of the bands. R_∞ is a fit parameter defined as $(I(0) - I(t))/\ I(0)$, $t_0$is the reaction starting time, k is the rate constant, and n is a parameter related to the dimensionality of the growth process. The main kinetics analysis relies on the n values, n<1 indicates a one-dimensional growth.[34] As shown in Fig. 5, the kinetic process at 25.5 GPa fitted well with the Avrami model. The fitted Avrami model of reacted 1,4-DFB shows n = 0.54, which indicates a linear growth of product, aligning with the formation of 1-D DNThs.

As discussed above, the product of 1,4-DFB propagates with a one-dimensional growth to form the fluoro-DNThs. However, the product still exhibited limited ordering, similar to that of benzene without slow compression.[35] Although the introduction of F atoms effectively modulates the molecular stacking and promotes a potential reaction pathway along the $[01\bar{1}]$ axis, it is not strong enough to alter the herringbone molecular stacking, thus resulting non-topochemical PIP like benzene.[5] In the future, designing a precursor with better molecular stacking in accordance with topochemical rules is also needed to be considered for synthesizing ordered, structure-specific products.

Conclusions

We investigated the high-pressure behaviour of 1,4-DFB through in situ Raman, IR spectroscopy, and XRD. Our findings revealed a phase transition around 12.0 GPa, and the onset of a reaction was demonstrated around 18.7 GPa. By investigating structure of product using SAED, a pseudo-hexagonal stacked fluoro-DNThs was demonstrated. Kinetic analysis of the reaction also supported one-dimensional growth, consistent with DNTh formation. By investigating the crystal structure of 1,4-DFB under high pressure and comparing it to that of benzene, we identified a potential reaction pathway along the $[01\bar{1}]$ axis for 1,4-DFB. This work underscores the potential of a bottom-up PIP approach for designing new carbon materials. By functionally modifying precursors and forming appropriate molecular stacking, it is anticipated that more carbon materials with predictable pathways and structures can be synthesized.

Author Contributions

The G. Che performed the experiments and theoretical calculations, wrote the original draft. Y. Wang and Z. Zhao helped to collect the XRD data. Y. Fei, T. Hattori and J. Abe helped to perform the in situ TOF neutron diffraction experiment. X. Tang and X. Dong helped to analyze the calculation results. X. Wang and J. Ju helped to collect the SAED data. Y. Wang, H. Zheng and K. Li led the entire experiment, data analysis, and manuscript writing. All authors approved the final version of the manuscript.

Conflicts of interest

There are no conflicts to declare.

Data availability

The data supporting this article have been included as part of the Supplementary Information.

Acknowledgements

The authors acknowledge the support of the National Key Research and Development Program of China (Grant Nos. 2023YFA1406200 and 2019YFA0708502), National Natural Science Foundation of China (Grant No. 22022101). In situ high-pressure X-ray diffraction experiments were performed at 4W2 beamline of Beijing Synchrotron Radiation Facility (BSRF). In situ high-pressure neutron diffraction experiment at the Materials and Life Science Experimental Facility of the J-PARC was performed through a user programs (Proposal No. 2023B0030). The authors thank Dr Dongliang Yang for supporting the in situ high-pressure X-ray diffraction experiments. This study was also partially supported by Synergic Extreme Condition User Facility (SECUF).

Notes and references

1. V. Schettino and R. Bini, *Chem. Soc. Rev.*, 2007, **36**, 869-880.
2. P. F. McMillan, *Chem. Soc. Rev.*, 2006, **35**, 855-857.
3. R. Bini, *Acc. Chem. Res.*, 2004, **37**, 95-101.
4. T. C. Fitzgibbons, M. Guthrie, E. S. Xu, V. H. Crespi, S. K. Davidowski, G. D. Cody, N. Alem and J. V. Badding, *Nat. Mater.*, 2015, **14**, 43-47.
5. X. Li, M. Baldini, T. Wang, B. Chen, E.S. Xu, B. Vermilyea, V. H. Crespi, R. Hoffmann, J. J. Molaison, C. A. Tulk, M. Guthrie, S. Sinogeikin and J. V. Badding, *J. Am. Chem. Soc.,* 2017, **139,** 16343-16349.
6. B. Chen, R. Hoffmann, N. W. Ashcroft, J. Badding, E. S. Xu and V. Crespi, *J. Am. Chem. Soc.,* 2015, **137**, 14373-14386.
7. P. Duan, X. Li, T. Wang, B. Chen, S. J. Juhl, D. Koeplinger, V. H. Crespi, J. V. Badding and K. Schmidt-Rohr, *J. Am. Chem. Soc.,* 2018*,* **140**, 7658-7666.
8. S. Huss, S. Wu, B. Chen, T. Wang, M. C. Gerthoffer, D. J. Ryan, S. E. Smith, V. H. Crespi, J. V. Badding and E. Elacqua, *ACS Nano.,* 2021, **15**, 4134-4143.

View Article Online
DOI: 10.1039/D4CP03751K

9. A. Biswas, M. D. Ward, T. Wang, L. Zhu, H.-T. Huang, J. V. Badding, V. H. Crespi and T. A. Strobel, *J. Phys. Chem. Lett.,* 2019, **10**, 7164-7171.
10. S. G. Dunning, L. Zhu, B. Chen, S. Chariton, V. B. Prakapenka, M. Somayazulu and T. A. Strobel, *J. Am. Chem. Soc.,* 2022, **144**, 2073-2078.
11. P. G. Demingos and A. R. Muniz, *J. Phys. Chem. C,* 2019, **123**, 3886−3891.
12. M. D. Ward, W. S. Tang, L. Zhu, D. Popov, G. D. Cody and T. A. Strobel, *Macromolecules,* 2019, **52**, 7557-7563.
13. A. Friedrich, I. E. Collings, K. F. Dziubek, S. Fanetti, K. Radacki, J. Ruiz-Fuertes, J. Pellicer-Porres, M. Hanfland, D. Sieh, R. Bini, S. J. Clark and T. B. Marder, *J. Am. Chem. Soc.,* 2020, **142**, 18907-18923.
14. M. C. Gerthoffer, S. Wu, B. Chen, T. Wang, S. Huss, S. M. Oburn, V. H. Crespi, J. V. Badding and E. Elacqua, *Chem. Sci.,* 2020, **11**, 11419-11424.
15. Y. Wang, X. Dong, X. Tang, H. Zheng, K. Li, X. Lin, L. Fang, G. Sun, X. Chen, L. Xie, C. L. Bull, N. P. Funnell, T. Hattori, A. Sano-Furukawa, J. Chen, D. K. Hensley, G. Cody, Y. Ren, H. H. Lee and H.-k. Mao, *Angew. Chem. Int. Edit.,* 2019, **58**, 1468-1473.
16. Y. Wang, L. Wang, H. Zheng, K. Li, M. Andrzejewski, T. Hattori, A. Sano-Furukawa, A. Katrusiak, Y. Meng, F. Liao, F. Hong and H.-k. Mao, *J. Phys. Chem. C*, 2016, **120**, 29510–29519.
17. H.-k. Mao, J. Xu and P. M. Bell, *J. Geophys. Res.*, 1986, **91**, 4673-4676.
18. C. Prescher and V. B. Prakapenka, *High Press. Res.,* 2015, **35**, 223-230.
19. T. Hattori, A. Sano-Furukawa, H. Arima, K. Komatsu, A. Yamada, Y. Inamura, T. Nakatani, Y. Seto, T. Nagai, W. Utsumi, T. Iitaka, H. Kagi, Y. Katayama, T. Inoue, T. Otomo, K. Suzuya, T. Kamiyama, M. Arai and T. Yagi, *Nuclear Instrum. Methods Phys. Res., Sect. A,* 2015, **780**, 55-67.
20. T. Hattori, A. Sano-Furukawa, S. Machida, J. Abe, K. Funakoshi, H. Arima and N. Okazaki, *High Press. Res.,* 2019, **39**, 417-425.
21. S. J. Clark, M. D. Segall, C. J. Pickard, P. J. Hasnip, M. I. J. Probert, K. Refson and M. C. Payne, *Z. Kristallogr*., 2005, **220**, 567-570.
22. J. P. Perdew and A. Zunger, *Phys. Rev. B*, 1981, **23**, 5048-5079.
23. F. Ortmann, F. Bechstedt and W. G. Schmidt, *Phys. Rev. B*, 2006, **73**, 205101.
24. M. M. Thiéry and J. M. Léger, *J. Chem. Phys.*, 1988, **89**, 4255-4271.
25. M. M. Rai, H. D. Bist and D. P. Khandelwal, *Appl. Spectrosc.,* 1971, **25**, 442-448.
26. V. R. Thalladi, H.-C. Weiss, D. Bläser, R. Boese, A. Nangia and G. R. Desiraju, *J. Am. Chem. Soc.,* 1998, **120**, 8702-8710.
27. F. Birch, *J. Geophys. Res.,* 1978, **83**, 1257−1268.
28. W. S. Tang and T. A. Strobel, *J. Phys. Chem. C,* 2020, **124**, 25062 −25070.
29. L. Ciabini, F. A. Gorelli, M. Santoro, R. Bini, V. Schettino and M. Mezouar, *Phys. Rev. B*, 2005, **72**, 094108.
30. A. D. Chanyshev, K. D. Litasov, S. V. Rashchenko, A. Sano-Furukawa, H. Kagi, T. Hattori, A. F. Shatskiy, A. M. Dymshits, I. S. Sharygin and Y. Higo, *Cryst. Growth Des.*, 2018, **18**, 3016−3026.
31. A. Bondi, *J. Phys. Chem.,* 1964, **68**, 441–451.
32. X. Li, T. Wang, P. Duan, M. Baldini, H.-T. Huang, B. Chen, S. J. Juhl, D. Koeplinger, V. H. Crespi, K. Schmidt-Rohr, R. Hoffmann, N. Alem, M. Guthrie, X. Zhang and J. V. Badding, *J. Am. Chem. Soc.,* 2018, **140**, 4969−4972.
33. S. J. Juhl, T. Wang, B. Vermilyea, X. Li, V. H. Crespi, J. V. Badding and N. Alem, *J. Am. Chem. Soc.,* 2019, **141**, 6937-6945.
34. S. Romi, S. Fanetti, F. Alabarse, A. M. Mio and R. Bini, *Chem. Sci.*, 2021, **12**, 7048–7057.
35. B. R. Jackson, C. C. Trout and J. V. Badding, *Chem. Mater.,* 2003, **15**, 1820-1824.

View Article Online
DOI: 10.1039/D4CP03751K

The data supporting this article have been included as part of the Supplementary Information.